Position Quadrature Measurements of a Nanomechanical Resonator Using Pulsed Optomechanics

Master's Thesis, 7.11.2023

Author:

Milla Männikkö

Supervisor:

Juha Muhonen
Arvind Kumar

UNIVERSITY OF JYVÄSKYLÄ
DEPARTMENT OF PHYSICS

Abstract

Männikkö, Milla
Master's thesis
Department of Physics, University of Jyväskylä, 2023, 50 pages.

As measurement technologies evolve, it becomes apparent that the limitations to measurement precision arise increasingly from the fundamental principles of quantum mechanics. Avoiding these limitations is however possible with a clever combination of techniques. In this thesis interferometric pulsed optomechanical measurement series were done on a nanobeam photonic crystal resonator to measure its position quadrature as measuring only one quadrature at a time allows for dodging the standard quantum limit. Resonator position was measured at an accuracy of 311 times the zero point fluctuation (x_{zpf}) of the resonator.

Keywords: optomechanics, quantum information, photonics

Tiivistelmä

Männikkö Milla
Pro gradu -tutkielma
Fysiikan laitos, Jyväskylän yliopisto, 2023, 50 sivua

Mittaustekniikan kehityksen myötä on ilmennyt, että tänä päivänä yhä useammin mittatarkkuutta rajoittavat kvanttimekaaniset ilmiöt. Tämä kvanttimekaniikan tuoma raja mittaustarkkuudelle voidaan kuitenkin väistää nokkelalla yhdistelmällä tekniikoita. Tässä pro gradu -tutkielmassa tehtiin pulssitettuja optomekaanisia mittaussarjoja fotonikiteiselle nanopalkkiresonaattorille sen paikkakvadratuurin mittamista varten, sillä vain toisen kvadratuurin mittaaminen mahdollistaa kvanttimekaniikan asettaman tarkkuusrajan välttämisen. Resonaattorin paikka mitattiin tarkuudella, joka oli 311 kertainen verrattuna resonaattorin nollapiste-energiassa tapahtuvaan värähtelyyn (x_{zpf}) verrattuna.

Avainsanat: Optomekaniikka, kvantti-informaatio, fotoniikka

Contents

1 Introduction

In optomechanics electromagnetic radiation and mechanical motion interact via radiation pressure causing interesting physical phenomena. One of the pioneers of optomechanics is Braginsky, who in his paper with Manukin [1] showed the theory and then later proved [2] that a mechanical oscillator can be heated or cooled via damping by radiation pressure. Braginsky also wrote papers about there being quantum mechanical limitations to how precisely oscillations can be measured [3]. This precision limit for interferometers was later analyzed by Caves [4]. These works established the standard quantum limit (SQL) for interferometers, a limit of how precisely the position of a free mass can be known and is a result of the Heisenberg uncertainty principle.

Already in Caves' paper in 1980 [4] it was suggested that the SQL can be avoided if squeezed light is used. While the SQL could be surpassed with this method, arbitrary measurement precision could not be reached. Arbitrarily precise measurements could bypass this limit by only measuring one observable at a time with pulsed light [5][6]. Measuring this one observable again before the state has decayed would yield the same result and hence not destroy the measured state, meaning that the measurements would also be quantum non-demolition (QND) measurements. In 1990 Jaekel and Reynaud [7] showed that correctly used squeezed light would indeed be able to achieve sensitivity beyond the SQL. In [6] it was shown that the SQL can't be evaded with continuous measurement.

Later it was theorized [8] and shown that light pulsed with pulse lengths much shorter than the mechanical oscillation period could actually be used for a full state tomography when used correctly [9][10]. It has also been shown that pulsed light can be used for cooling [9] and coherent quantum memory [11]. As such, pulsed optomechanics has been shown to be a good approach to studying quantum mechanical systems.

In this thesis I have analyzed pulsed optomechanical measurement series on the position observable of a mechanical resonator and got the result that the resonator's position was measured at a precision of 311 x_{zpf}. As this precision has been achieved

in room temperature it seems that reaching precisions close to x_{zpf} should be manageable at liquid Helium temperatures.

2 Theoretical background

In the measurements done for this thesis, an interferometric optomechanical setup where a laser beam measures the vibrations of a mechanical resonator via its coupling to an optical cavity was used. As the mechanical resonator is coupled to an optical cavity, the optomechanical interaction between light and the mechanical resonator changes the phase of the light coming out from the cavity. This change of phase is then interferometrically measured as it interferes with a laser beam that has not gone through the cavity. As only one laser is used i.e. the source of the light going to the cavity arm of the interferometer is the same as the source of the light in the reference arm (called local oscillator), this measurement is a homodyne measurement.

The laser light used for measuring the optomechanical interaction can be continuous or pulsed. In the measurements done for this thesis, pulsed light with pulse lengths much shorter than the mechanical oscillation period was used. This was due to multiple reasons with the most important motivation being that using pulsed light allows for bypassing the Heisenberg uncertainty principle that limits the measurement precision of quantum measurements as discussed in Sec. 1. This will be discussed in more detail in Sec. 2.5. Pulsed light also has other benefits such as being a faster measurement method than continuous light for sensing small frequency changes of the mechanical oscillator. A more detailed explanation for choosing pulsed light over continuous light will be included later in this section.

In the following subsections, I will explain the theoretical background of the measurement system. I start by explaining cavity optomechanics relevant to this system and give a brief definition for quadratures. After that, I explain how the laser detuning results in a phase shift in the cavity arm (called signal arm) of the interferometer and how radiation pressure causes optomechanical coupling. Next, I will discuss the details of homodyne measurements, how quadratures are measured, and define backaction. Lastly, I discuss how measurement precision is extracted and the advantages of doing pulsed measurements over continuous measurements when measuring quadratures. I also briefly explain how the measurement results are deciphered, a more in-depth description of the analysis done to the measurement

data can be found in Sec. 4.1.

2.1 Cavity optomechanics

The measurement system used consists of a mechanical resonator coupled to an optical cavity in such a way that the position of the resonator changes the cavity resonance frequency. The resonator can then be coupled to other things such as a spin, for example, affecting the resonator's mechanical resonance frequency. Thus this makes the thing coupled to the mechanical resonance detectable as a change in the optical resonance. While the cavity studied in this thesis is not a Fabry-Perot cavity, the physical properties of the cavity used are similar enough that most equations for a Fabry-Perot cavity hold for this cavity as well [12].

2.1.1 Optical cavity physics

In an optical cavity there are two or more mirrors between which light gets reflected. Let's start by considering a simple cavity of two mirrors where one of the mirrors can move and one is at a fixed position. These mirrors have transmissions t_1 and t_2 and reflectivities r_1 and r_2. The amount of light that goes through a cavity without getting scattered or absorbed is called transmittance. For the cavity described here the transmittance T is [13] [14]

$$T = |t|^2 = \frac{|t_1 t_2|^2}{|1 - r_1 r_2 e^{-i2\phi}|^2} \tag{1}$$

where ϕ is the phase that the light gathers while travelling between the mirrors in the cavity. The phase is thus dependent on the distance between the cavity mirrors L [14]

$$\phi = \frac{L\omega}{c} = nkL, \tag{2}$$

where ω is the frequency of the light, n is the refractive index of the mirrors and k is the wave number. Setting $\phi = \pi$ one gets the equation for free spectral range frequency ω_{FSR} [14]

$$\omega_{FSR} = \frac{\phi c}{L} = \frac{\pi c}{L} \tag{3}$$

The free spectral range yields the difference in frequency between two cavity resonances ω_{cav} [15]. Thus one can define the cavity resonance as

$$\omega_{cav} = p\omega_{FSR} = p\frac{\pi c}{L}, \tag{4}$$

where p is the cavity mode integer.

The optics of this cavity can be described as a harmonic oscillator thus meaning that one can write a Hamiltonian that describes the cavity's optical properties as

$$H = \hbar\omega_{cav}(\hat{a}^\dagger\hat{a} + \frac{1}{2}) \tag{5}$$

where [15] $\hat{a}^\dagger$ and $\hat{a}$ are the creation and annihilation operators for photons, with $\hat{a}^\dagger\hat{a}$ being the number of photons circulating in the cavity.

2.1.2 Mechanical resonator

As stated at the start of the previous subsection, the cavity has a moving mirror. If this mirror moves at a mechanical oscillation frequency Ω_m, then it will change the length L of the optical cavity and thus change the cavity resonance frequency ω_{cav} as can be seen from eq. 4. Assuming that the moving mirror behaves mostly like a harmonic oscillator, its movement when acted upon by some sum of external forces F_e can be described with the following equation [15]

$$m_{eff}\frac{dx^2(t)}{dt^2} + m_{eff}\Gamma_m\frac{dx(t)}{dt} + m_{eff}\Omega_m^2 x(t) = F_e x(t) \tag{6}$$

where m_{eff} is the effective mass of the harmonic oscillator, $x(t)$ is the position of the oscillator as a function of time t and Γ_m is the damping of the oscillator that is assumed to be frequency independent here.

As before with the cavity's oscillation being described as a harmonic oscillator, one can also describe the mechanical resonator as a harmonic oscillator. The Hamiltonian for the mechanical resonator can be written as [15]

$$H = \hbar\Omega_m(\hat{b}^\dagger\hat{b} + \frac{1}{2}) \tag{7}$$

where $\hat{b}^\dagger$ and $\hat{b}$ are the creation and annihilation operators for phonons in the resonator and where driving and damping have not been accounted for. As these are ladder

operators, these can be used to define the position and momentum operators $\hat{x}$ and $\hat{p}$:

$$\hat{x} = \sqrt{\frac{\hbar}{2m_{eff}\Omega_m}}(\hat{b} + \hat{b}^\dagger), \tag{8}$$

$$\hat{p} = i\sqrt{\frac{\hbar m_{eff}\Omega_m}{2}}(\hat{b}^\dagger - \hat{b}). \tag{9}$$

The position and momentum operators can also be defined with the use of the zero point fluctuation of the mechanical resonator x_{zpf} [15],

$$x_{zpf} = \sqrt{\frac{\hbar}{2m_{eff}\Omega_m}} \tag{10}$$

yielding the following equations for the operators

$$\hat{x} = x_{zpf}(\hat{b} + \hat{b}^\dagger), \tag{11}$$

$$\hat{p} = im_{eff}\Omega_m x_{zpf}(\hat{b}^\dagger - \hat{b}). \tag{12}$$

As position and momentum are non-commuting operators, they can be considered quadrature operators as I will next define.

2.2 Quadratures

Quadrature operators are defined as two non-commuting dimensionless operators [16]. The two non-commuting observables for the system studied can be for example the mechanical observables position and momentum, and in that case, the quadrature operators for these observables are called position quadrature and momentum quadrature. Similarly, the optical observables phase and amplitude can have quadrature operators which would then be called phase quadrature and amplitude quadrature.

The general mathematical definition for two quadrature operators $\hat{X}$ and $\hat{Y}$ can be written as [16]

$$\hat{X}(t) = \frac{1}{\sqrt{2}}(\hat{c}^\dagger e^{i\omega t} + \hat{c}e^{-i\omega t}) = \hat{x}_1^{\omega t} \tag{13}$$

$$\hat{Y}(t) = \frac{i}{\sqrt{2}}(\hat{c}^\dagger e^{i\omega t} - \hat{c}e^{-i\omega t}) = \hat{x}_2^{\omega t} \tag{14}$$

where t is time, $\hat{c}^\dagger$ and $\hat{c}$ are creation and annihilation operators relating to $\hat{x}_1$ and $\hat{x}_2$ in a frame rotating at frequency ω. These operators are non-commuting observable operators like position and momentum or phase and amplitude or like $\hat{X}$ and $\hat{Y}$.

2.3 Laser detuning and optomechanical coupling

So far the cavity has been considered from an optical and a mechanical point of view. However, as the optics and the mechanics are coupled, it is necessary to understand the system as an optomechanical system where the optics affect the mechanics and vice versa.

If the oscillating mirror is only ever slightly displaced, the cavity resonance frequency ω_{cav} can be expressed as a function of displacement x [12][13]

$$\omega_{cav}(x) \approx \omega_{cav} + x\frac{\partial\omega_{cav}}{\partial x} + \frac{1}{2}x^2\frac{\partial^2\omega_{cav}}{\partial x^2} + ... \tag{15}$$

In the system studied for this thesis, only the linear $x\frac{\partial\omega_{cav}}{\partial x}$ term contributes in a significant way, meaning that $\omega_{cav}(x)$ can be approximated as [12][15]

$$\omega_{cav}(x) \approx \omega_{cav} + x\frac{\partial\omega_{cav}}{\partial x}. \tag{16}$$

Thus it is reasonable to define the coupling between the optical and mechanical oscillation as

$$G = -\frac{\partial\omega_{cav}}{\partial x}, \tag{17}$$

where G is the amount of shift in optical frequency in relation to the displacement of the mirror [15].

The Hamiltonian of the system, if the optics and mechanics are not coupled but independent of each other, can be defined as a sum of the optical Hamiltonian in eq. 5 and mechanical Hamiltonian in eq. 7

$$H = \hbar\omega_{cav}(\hat{a}^\dagger\hat{a} + \frac{1}{2}) + \hbar\Omega_m(\hat{b}^\dagger\hat{b} + \frac{1}{2}). \tag{18}$$

To simplify equations from here on, the 1/2 terms are left out from the Hamiltonian, as it does not affect the equations other than offset them the amount of ground state

energy [12]. Plugging eq. 17 into 16 allows accounting for the coupling and yields

$$\omega_{cav}(x) \approx \omega_{cav} - \hat{x}G, \tag{19}$$

to which eq. 8 can be plugged into yielding

$$\omega_{cav}(x) = \omega_{cav} - Gx_{zpf}(\hat{b} + \hat{b}^\dagger). \tag{20}$$

Since optomechanical coupling strength is defined as [15]

$$g_0 = x_{zpf}G, \tag{21}$$

the Hamiltonian in eq. 18 can now be written as

$$H = \hbar(\omega_{cav} - g_0(\hat{b} + \hat{b}^\dagger))\hat{a}^\dagger\hat{a} + \hbar\Omega_m\hat{b}^\dagger\hat{b} \tag{22}$$

$$= \hbar\omega_{cav}\hat{a}^\dagger\hat{a} - \hbar g_0\hat{a}^\dagger\hat{a}(\hat{b} + \hat{b}^\dagger) + \hbar\Omega_m\hat{b}^\dagger\hat{b} \tag{23}$$

where the first term is the photon energy, the second term is the interaction term [12][15] and the last term is the phonon energy.

2.3.1 Laser detuning

As was explained in the description of the system, there is a laser beam going into the cavity. If the cavity resonance frequency differs from the frequency of the laser beam light, there will be a frequency difference $\Delta_0 = \omega_L - \omega_{cav}$ between them, where ω_L is the frequency of the laser beam. This frequency difference is called detuning.

In the eq. 23 the Hamiltonian for the optomechanical system was defined without consideration for the frequency of the light coming in to the cavity. This frequency difference can be accounted for by considering this system rotating at the laser frequency ω_L [15][16]. The Hamiltonian will thus now be defined as

$$H = \hbar\Delta_0\hat{a}^\dagger\hat{a} - \hbar g_0\hat{a}^\dagger\hat{a}(\hat{b} + \hat{b}^\dagger) + \hbar\Omega_m\hat{b}^\dagger\hat{b}, \tag{24}$$

where all terms concerning decay, fluctuation and driving have been left out.

Let's say that the electromagnetic field inside the cavity has amplitude $\hat{a}$. Using input-output theory, the change of amplitude $\hat{a}$ as a function of time can be written

as [10]

$$\frac{d\hat{a}}{dt} = -\frac{\kappa}{2}\hat{a} + i\Delta(t)\hat{a} + \sqrt{\kappa_{ex}}\hat{a}_{in}, \tag{25}$$

where $\Delta(t) = \Delta_0 + Gx(t)$ is the modified detuning where the movement of the resonator is taken into account in the detuning, $\kappa = \kappa_{ex} + \kappa_0$ is the photon decay rate, κ_{ex} is the rate of photon decay caused by the Fabry-Perot cavity input mirror, κ_0 is the photon decay rate from things inside the cavity such as scattering and absorption and $\hat{a}_{in}$ is the complex amplitude of the cavity input field. Assuming that the amplitude is at a steady state i.e. $\frac{d\hat{a}}{dt} = 0$, the amplitude $\hat{a}$ can be solved from eq. 25 to be [15][10]

$$\hat{a} = \frac{\sqrt{\kappa_{ex}}\hat{a}_{in}}{\frac{\kappa}{2} - i\Delta(t)}. \tag{26}$$

From the above equation it can be seen that the changes in the electromagnetic wave are from the detuning i.e. the phase change the light experiences in the cavity is due to the detuning.

2.3.2 Radiation pressure

Radiation pressure is the position operator derivative of the interaction Hamiltonian in eq. 23 [15]

$$F_{rp} = -\frac{\partial}{\partial\hat{x}}\left(-\hbar g_0 \hat{a}^\dagger\hat{a}(\hat{b} + \hat{b}^\dagger)\right) \tag{27}$$

where F_{rp} is the radiation pressure force. Since the photon creation and annihilation operators are not related to the position operator one gets that

$$\begin{aligned}
F_{rp} &= \hbar\hat{a}^\dagger\hat{a}\frac{\partial}{\partial\hat{x}}\left(g_0\hat{b} + g_0\hat{b}^\dagger\right) && (28)\\
&= \hbar\hat{a}^\dagger\hat{a}\frac{\partial}{\partial\hat{x}}\left(x_{zpf}G\hat{b} + x_{zpf}G\hat{b}^\dagger\right) && (29)\\
&= \hbar G\hat{a}^\dagger\hat{a}\frac{\partial}{\partial\hat{x}}\left(\frac{\hat{x}}{\hat{b}+\hat{b}^\dagger}\hat{b} + \frac{\hat{x}}{\hat{b}+\hat{b}^\dagger}\hat{b}^\dagger\right) && (30)\\
&= \hbar G\hat{a}^\dagger\hat{a} && (31)\\
&= \hbar\frac{g_0}{x_{zpf}}\hat{a}^\dagger\hat{a}. && (32)
\end{aligned}$$

In section 2.1.2 an equation for the motion of the mechanical resonator was introduced in eq. 6. The radiation pressure force from the laser beam in the cavity is one of if not the only external force acting on the mechanical resonator. As such it is easy to

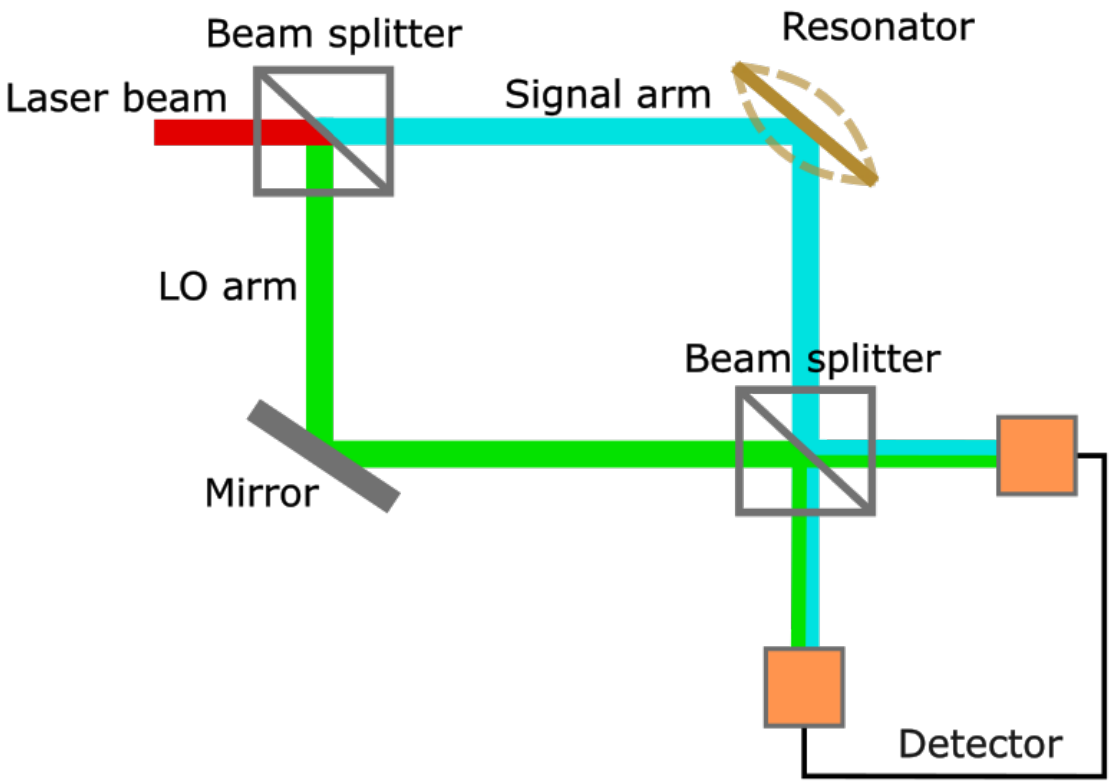

Figure 1. A schematic picture of a Mach-Zender interferometer.

see that the radiation pressure affects the mechanical resonator thus coupling the optics and mechanics of the cavity.

2.4 Homodyne measurements

In the measurement setup the oscillations are read interferometrically. A simplified schematic of the setup is in figure 1.

The laser light is first split by a 50/50 beamsplitter to go to the LO (local oscillator) and the signal arms of the interferometer. Both of these arms are the same length if the resonator sample is not oscillating or is replaced with a mirror. Light sent to the LO arm goes straight to the detector whereas the light sent to the signal arm enters and exits the optical cavity and after that goes to the detector. Before hitting the detector, the light coming from both of these arms interferes in a beamsplitter, after which the interfered light of both arms is sent to both detector eyes.

When the beams from the different arms interfere, the resultant light's intensity depends on the phase difference between the arms as the resulting beam's amplitude is the sum of the two beam amplitudes due to superposition. As the light sent to the LO arm of the interferometer experiences no changes to phase, it can be thought of as a control for how much the phase has changed in the signal arm. What is then actually measured at the detector is the intensity of the interfered light. This intensity is then digitized into voltage in the detector so that the voltage V measured by the detector is proportional to the homodyne signal S i.e. $V \propto S$. Next, I will show the derivation of the homodyne signal S.

The signal beam and the LO beam will have complex amplitudes A_s and A_{LO} at the beamsplitter before the last beamsplitter. These two beams will interfere at the beamsplitter and then be split into two different beams and sent to the detector eyes. The amplitudes of these two new beams after the splitter will be [13] $A_+ = 1/\sqrt{2}(A_s + A_{LO})$ and $A_- = 1/\sqrt{2}(-A_s + A_{LO})$. The optical powers of these amplitudes will be measured in the detector eyes and subtracted from each other. This value will then be turned into a voltage value that will be proportional to the intensity of the interfered light as mentioned before. The homodyne signal S can be defined as [10]

$$
\begin{aligned}
S &= |A_+|^2 - |A_-|^2 && (33)\\
&= |1/\sqrt{2}(A_s + A_{LO})|^2 - |1/\sqrt{2}(-A_s + A_{LO})|^2 && (34)\\
&= \frac{1}{2}(|A_s + A_{LO}|^2 - |-A_s + A_{LO}|^2) && (35)\\
&= \frac{1}{2}\left[(A_s + A_{LO})^*(A_s + A_{LO}) - (-A_s + A_{LO})^*(-A_s + A_{LO})\right] && (36)\\
&= A_s^* A_{LO} + A_s A_{LO}^* && (37)
\end{aligned}
$$

For these measurements the complex signal amplitude A_s is $\sqrt{\kappa_{out}}\hat{a}$, where $\hat{a}$ is defined in the equation 26 and A_{LO} is $|A_{LO}|e^{i\theta}$, where θ is the phase difference between signal and LO amplitudes A_s and A_{LO} [10]. Plugging these into the equation

37 one gets

$$S = \left(\frac{2\sqrt{\kappa_{out}\kappa_{ex}}}{\kappa} \frac{\hat{a}_{in}(1 - i\frac{2\Delta}{\kappa})}{1 + (\frac{2\Delta}{\kappa})^2} |A_{LO}| e^{i\theta} + \frac{2\sqrt{\kappa_{out}\kappa_{ex}}}{\kappa} \frac{\hat{a}_{in}(1 + i\frac{2\Delta}{\kappa})}{1 + (\frac{2\Delta}{\kappa})^2} |A_{LO}| e^{-i\theta} \right) \tag{38}$$

$$= \frac{2\sqrt{\kappa_{out}\kappa_{ex}}}{\kappa} \frac{\hat{a}_{in}|A_{LO}|}{1 + (\frac{2\Delta}{\kappa})^2} \left((1 - i\frac{2\Delta}{\kappa}) e^{i\theta} + (1 + i\frac{2\Delta}{\kappa}) e^{-i\theta} \right) \tag{39}$$

$$= \frac{2\sqrt{\kappa_{out}\kappa_{ex}}}{\kappa} \frac{\hat{a}_{in}|A_{LO}|}{1 + (\frac{2\Delta}{\kappa})^2} \Bigg(\cos\theta + i\sin\theta - i\frac{2\Delta}{\kappa}\cos\theta + \frac{2\Delta}{\kappa}\sin\theta$$

$$+ \cos\theta - i\sin\theta + i\frac{2\Delta}{\kappa}\cos\theta + \frac{2\Delta}{\kappa}\sin\theta \Bigg) \tag{40}$$

$$= \frac{2\sqrt{\kappa_{out}\kappa_{ex}}}{\kappa} \frac{\hat{a}_{in}|A_{LO}|}{1 + (\frac{2\Delta}{\kappa})^2} \left(2\cos\theta + \frac{4\Delta}{\kappa}\sin\theta \right) \tag{41}$$

$$= \frac{4\sqrt{\kappa_{out}\kappa_{ex}}}{\kappa} |A_{LO}| \frac{\hat{a}_{in}}{1 + (\frac{2\Delta}{\kappa})^2} \left(\cos\theta + \frac{2\Delta}{\kappa}\sin\theta \right). \tag{42}$$

From the equation 42 one can see the homodyne signal's dependence on the phase difference between the two interferometer arms. If the phase difference between them is $\theta = 0$, then only the field amplitudes matter. The phase of the light that went to the cavity has either not changed at all or only changed by $2n\pi$, where n is an integer. It is also true that only the field amplitudes matter when the phase changes $n\pi$, however, this phase change also causes the sign of the signal to flip.

If the phase difference is other than 0 or π the homodyne signal is sensitive to detuning. More specifically if the phase difference is $\theta = \pi/2$, the signal is linearly dependent on the detuning [10]. Since in this case detuning is caused by the change in cavity length, the phase difference bestows information about the amount of detuning and thus about the position of the mechanical oscillator. At this phase difference

$$S \propto \frac{\frac{2\Delta(t)}{\kappa}}{(\frac{2\Delta(t)}{\kappa})^2 + 1}. \tag{43}$$

When doing these measurements with laser frequency at the optical resonance frequency i.e. $\omega_L = \omega_{cav}$ and thus $\Delta_0 = 0$, the modified detuning is $\Delta(t) = Gx(t)$ and the previous proportionality can be written as

$$S \propto \frac{\frac{2G}{\kappa}x(t)}{(\frac{2Gx(t)}{\kappa})^2 + 1}. \tag{44}$$

From this equation it is apparent, that as long as $\frac{2Gx(t)}{\kappa} \ll 1$ is true, the equation is

linear. Unfortunately this is not always the case for the measurements done in this thesis and thus some measurements were nonlinear.

2.5 Measuring quadratures and avoiding backaction

Quadratures can be measured and as they can be defined by the position and momentum operator, measuring them can yield information about the position or momentum of a mechanical oscillator. The position of a mechanical resonator can, for example, be written as [10] [15]

$$\hat{x}(\theta) = \hat{X}\cos(\theta) + \hat{Y}\sin(\theta) \tag{45}$$

where $\hat{x}(\theta)$ is the position of a mechanical resonator as a function of the angle $\theta = \Omega_m t$ and $\hat{X}$ and $\hat{Y}$ are quadrature amplitudes. From eq. 45 one sees that at $t = 0$

$$\hat{x}(0) = \hat{X} \tag{46}$$

It is also known that [15]

$$\hat{Y} = \frac{\hat{p}(0)}{m_{eff}\Omega_m} \tag{47}$$

Since the position and momentum operators' commuting relation is $[\hat{x},\hat{p}] = i\hbar$, then for the quadrature operators the commutation relation is

$$[\hat{X},\hat{Y}] = \hat{X}\hat{Y} - \hat{Y}\hat{X} \tag{48}$$

$$= \hat{x}(0)\frac{\hat{p}(0)}{m_{eff}\Omega_m} - \frac{\hat{p}(0)}{m_{eff}\Omega_m}\hat{x}(0) \tag{49}$$

$$= \frac{[\hat{x}(0),\hat{p}(0)]}{m_{eff}\Omega_m} \tag{50}$$

$$= \frac{i\hbar}{m_{eff}\Omega_m}. \tag{51}$$

Plugging equation 51 into the Heisenberg uncertainty principle one gets [5] [15]

$$\Delta X \Delta Y \geq \frac{1}{2}\left|\left\langle\left[\hat{X},\hat{Y}\right]\right\rangle\right| \tag{52}$$

$$\implies \Delta X \Delta Y \geq \frac{1}{2}\left|\left\langle \frac{i\hbar}{m_{eff}\Omega_m}\right\rangle\right| \tag{53}$$

$$\implies \Delta X \Delta Y \geq \frac{\hbar}{2m_{eff}\Omega_m} \tag{54}$$

$$\implies \Delta X \Delta Y \geq x_{zpf}^2, \tag{55}$$

where ΔX and ΔY are the standard deviations of the observables X and Y. From the previous equation, it is clear to see, that measuring both ΔX and ΔY at the same time will yield at least imprecision of amount x_{zpf}^2 [5]. Thus the standard quantum limit (SQL) can't be avoided in this sort of measurement. However, if one were to only measure one of these quadratures at a time, then in theory it should be possible to measure it as precisely as one wants.

2.5.1 Backaction

The mechanical motion of the resonator causes the cavity length to vary in time thus changing the optical resonance frequency. A change in the optical resonance frequency then changes the radiation pressure force that the mechanical resonator experiences, as the radiation pressure force is dependent on the optical resonance frequency. Similarly, if there is a fluctuation in the radiation pressure force that the resonator experiences, it affects the resonator's mechanical motion. In both cases, there is a feedback loop. This disturbance feedback loop that measuring with light causes is called backaction [15]. The unavoidable quantum fluctuation in the radiation pressure force enforces a limit to how precisely measurements can be done and thus if possible, one wants to avoid this limit.

2.6 Extracting measurement noise

As will be discussed in more detail in Sec. 2.7.1, measurements in this thesis are done as pulses that are either separated by half of the mechanical oscillation period of the resonator or by the full oscillation period. Measuring with pulses half a period apart yields the quadrature amplitude whereas measuring at full periods yields the noise of the measurements. This will be shown in Sec. 2.7.1. While calculating the exact precision of the measurement might be difficult, it is possible to calculate the amount of noise in the measurement from the amount of noise variance compared to thermal variance in terms of x_{zpf}.

When the resonator is at thermal equilibrium, the normalized resonator position $x_n = x/x_{zpf}$ will have a probability density that is Gaussian [10]. Thus it will have variance

$$\mathrm{Var}(x_n) = \frac{2k_BT}{\hbar\omega_m} = 2n_{th} \tag{56}$$

where k_B is the Boltzmann constant, T is the resonator temperature, $\hbar$ is the Planck constant and n_{th} is the number of thermal phonons in the cavity. Similarly, the thermal variance or the variance of the measured quadratures is [10]

$$\mathrm{Var}(X) = 2n_{th}x_{zpf}^2 \tag{57}$$

where X is the quadrature amplitude measured.

As mentioned, the difference in the pulses that are a full oscillation period apart measure the shot noise of the system and thus taking a variance of such measurement would yield the variance of the shot noise. This variance can then be stated in terms of x_{zpf} the following way

$$\frac{\mathrm{Var}(x_{2\pi})}{x_{zpf}^2}, \tag{58}$$

where $\mathrm{Var}(x_{2\pi})$ is the variance of the shot noise measurement. Solving for x_{zpf} in eq. 57 and plugging it into eq. 58 one gets

$$\sqrt{\frac{\mathrm{Var}(x_{2\pi})}{x_{zpf}^2}} = \sqrt{\frac{\mathrm{Var}(x_{2\pi})2n_{th}}{\mathrm{Var}(X)}}, \tag{59}$$

which reveals the measurement precision.

2.7 Benefits of using pulsed light in quadrature measurement

Backaction is one of the many reasons why using pulsed light is preferable to continuous light: if one puts continuous light in the cavity, there will constantly be a radiation pressure on the mechanical resonator. This will cause the backaction loop to stay online as long as there is light going to the cavity faster than the light decays out of the cavity. If the light going to the cavity is pulsed, the backaction can be somewhat evaded as long as the pulse duration is much less than the mechanical oscillation period [8].

Based on eq. 45, continuously measuring θ would measure both $\hat{X}$ and $\hat{Y}$ quadratures thus causing the measurement precision to be limited by the SQL. Using pulsed measurements and only measuring at $\theta = n\pi$ for example would however only ever measure the $\hat{X}$ thus avoiding the SQL. This is one downside of using pulsed light: only one quadrature can be measured at a time.

There is, however, an advantage in measuring only one quadrature at a time: the noise caused by the measurement only goes to the quadrature not measured [8][10]. If only X quadrature, which is the position or phase quadrature, is measured, then measurements are done only at angles $\theta = 0, \pi, ..., n\pi$, where n is an integer. The radiation pressure force applied to the resonator changes the resonator's momentum but not the frequency it's oscillating at. Thus the effect of the radiation pressure goes to the amplitude. As the frequency stays the same, after a full period of oscillation the resonator will be at the same point of oscillation as it would have been if no radiation pressure force was applied. Avoiding measurement noise like this is the most important advantage of using pulsed light in these measurements.

If the mechanical resonator's resonance frequency is less than the cavity decay rate κ i.e. $\Omega_m \ll \kappa$, then the detuning and thus phase shift θ that the photons in the cavity get is [15]

$$\theta \propto \frac{Gx}{\kappa} \tag{60}$$

When using the photons passing through the cavity to measure this phase shift, the photons will only have shot noise of [15]

$$\delta\theta = \frac{1}{\sqrt{N}} \tag{61}$$

where $\delta\theta$ is the noise and N is the number of photons going through the cavity. Thus

the more photons pass through the cavity the less shot noise we'll have. This is however only true for short and intense laser pulses [15], as the light inflicts radiation pressure on the mechanical resonator leading to more uncertainty.

2.7.1 Pulsed measurement results

As has already been described, the phase difference of light between two interferometer arms is measured. The light sent to both interferometer arms is pulsed so that light goes to the arms only at times that are half of the mechanical oscillation period apart (π measurements) or a full mechanical oscillation period apart (2π measurements). There is only a minimal amount of light going to the arms when there is no pulse. These pulsed measurements result in voltage data that can be plotted as a function of time. Such plots show that there are peaks in the voltage at the times of the pulses. These peaks can then be analyzed to find out what the position of the resonator at the instance of the laser pulse averaged over the pulse duration was. As was established at the beginning of section 2.4, the measured voltage is proportional to the homodyne signal. The homodyne signal is proportional to the position of the mechanical resonator $x(t)$, meaning that during a pulse, the area under a peak corresponds with the position of the mechanical resonator.

As a measurement will always have noise, some amount of the area under the peak is due to measurement noise. I will next discuss how the quadrature amplitudes can be solved from the areas under the peaks and how the amount of noise for these measurements was determined.

If the mechanical resonator's position is measured first at $t = 0$ and again after half of an oscillation period has passed, the measured quadrature amplitudes are X and $-X$. Thus the difference of the area under pulses measured at these times should yield $X - (-X) = 2X$. Measuring both X and $-X$ helps to cancel out offset noise from the measurement. As $x_\pi = \frac{X-(-X)}{2}$, it is clear that measuring the resonator with this pulse interval yields information about the resonator's position.

If the mechanical position is also measured at $t = 0$ and again after a full oscillation period has passed, the measured quadrature amplitudes are X and X. Taking the difference of the area under pulses at these times should yield $X - X = 0$. However, since there is always some random noise in the measurement, the difference between these areas won't be exactly zero, but the measurement noise. As $x_{2\pi} = \frac{(X+\delta_1)-(X+\delta_2)}{2} = \frac{\delta_1-\delta_2}{2}$, it's clear that nothing of the position or the offset

noise is kept thus leaving only shot noise. Doing measurements on the mechanical resonator at these pulse intervals will thus yield the shot noise of the measurement which can be used in the analysis of the measurement as it was explained in Sec. 2.6.

3 Methods and materials

In this section, I will describe the resonator used in this measurement and the fabrication details of it in Sec. 3.1, describe the system used to do the measurement in Sec. 3.2, and how control of the phase difference or the lack of such control affects this measurement in Sec. 3.3.

3.1 Nanobeam resonator properties and fabrication

All measurement results in this thesis were obtained from a photonic crystal nanobeam made of silicon that was sliced in the middle and clamped at both ends. These nanobeams are situated on a silicon chip in eight blocks. There are also multiple rectangular holes at and around the ends of the beam, these are present in the design to lessen the compressive strain on the resonator, which would otherwise affect the performance of the resonator [17]. An image of a nanobeam from the same block as the measured nanobeam taken with an electron microscope is in Fig. 2. These sorts of nanobeam structures have been shown to be able to have good optomechanical coupling [17][18] which is one of the reasons why they are being used in this research group.

A photonic crystal is a structure with periodically changing refractive index [14]. In the sliced nanobeam used in the measurements the refractive index changes due to there being holes at periodical distances in the beam. The patterning making this beam a photonic crystal is introduced to confine the light to the resonator [17]. The beam is sliced in the middle lengthwise to allow the beamhalves to move with respect to each other. As light goes to the optical cavity formed by the photonic crystal, the radiation pressure exerts a force on the resonator, that affects the resonator's motion. The resonator's mechanical resonance frequency was 1.95 MHz.

The resonator used in the measurements analyzed in this thesis is on a silicon chip with multiple other resonators. The chip has three layers in order from the bottom, a silicon layer, a silicon oxide layer, and another silicon layer. A layer of PMMA (polymethyl methacrylate) is applied on top of this for patterning, which is

done in an electron microscope with a dosage of 145 µC/cm^2, acceleration voltage of 20 kV, and an aperture of 30 µm with a 50 µm writefield. After patterning, the chip is developed to remove the PMMA in the shape of the pattern to have a mask for etching the silicon.

Next, the chip is dry-etched with ICP-RIE (Inductively Coupled Plasma-Reactive Ion Etcher) to remove silicon on the topmost layer in the shape of the mask. Lastly, the chip is wet etched with hydrogen fluoride for 3 minutes to release the structure. The wet etching etches the silicon oxide between the two layers of silicon so that the resonator is suspended over the bottom silicon layer. After the wet etching, the chip is transferred through 4 baths of deionized water into a critical point dryer. This has been proven to help with avoiding stiction [19]

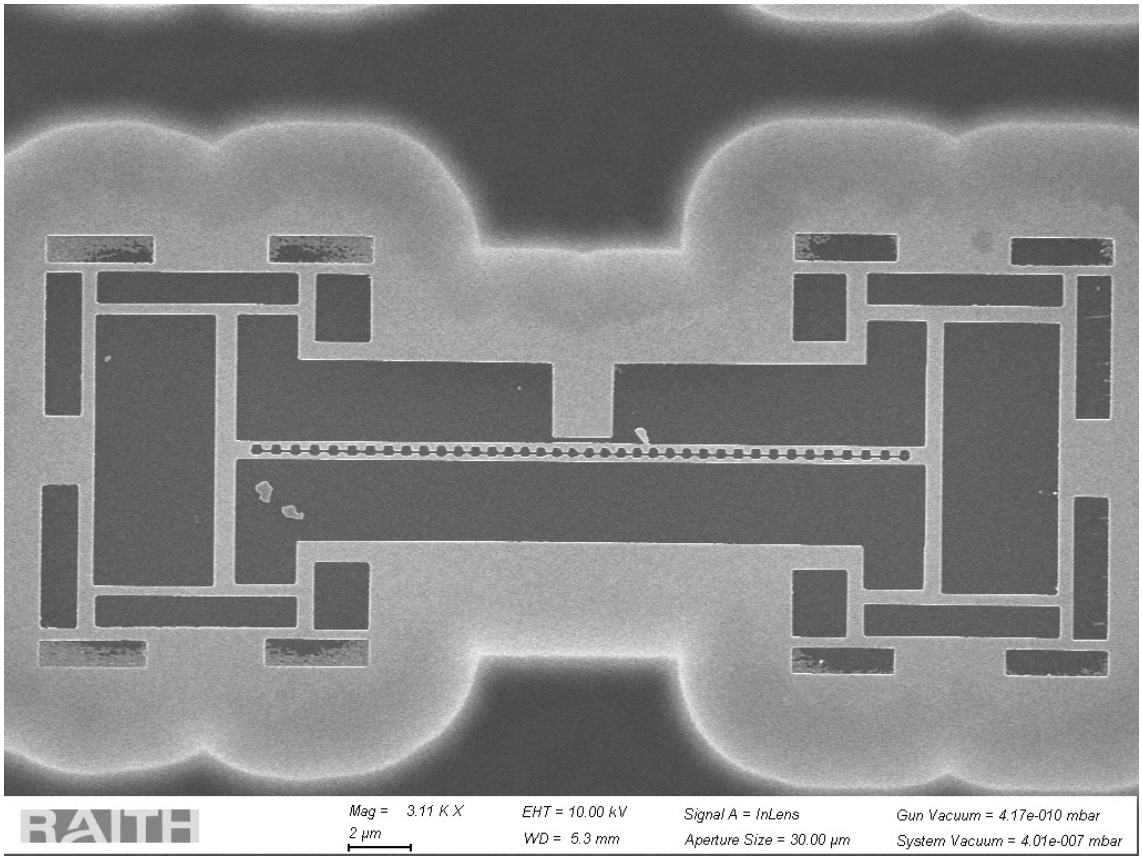

Figure 2. An image taken with an electron microscope of a nanobeam resonator. The area in lighter grey is the topmost layer of silicon while the lowest layer that the beam is suspended over is in darker grey. This is not the same resonator as was measured but it has the same design and was made on the same fabrication round as the resonator used in the measurements. The resonator itself is the thin beam split in the middle with square-like holes. The other, much bigger holes at the left and right ends of the resonator are made to lessen compressive strain on the resonator. The sample has a balcony above the resonator where a magnet could be, however, this nor the measured resonator had a magnet by design. There is also some unintended debris on this sample that was not present on the measured sample. The resonator and the image are by Cliona Shakespeare.

3.2 Measurement system

A simplified diagram of the measurement setup is shown in Fig. 3. The measurement system consists of a laser that goes to two interferometer arms: the signal arm, which goes to the sample in a vacuum chamber at room temperature and after interacting with the resonator, to the detector, and the LO arm, which goes straight to the detector. The laser is linearly polarized and split into these two arms via a fiber. In both arms, there are neutral density filters (referred to as ND filters from here forward) that lessen the light's intensity a certain amount for all wavelengths of light to make sure that there is not too much intensity going to either the resonator, as it can break, or to the detector, as it can saturate or break.

To pulse the laser, the laser going to the arms goes through an EOM (electro-optic modulator), which controls the light's intensity based on a bias voltage. The bias voltage is sent from an AWG (arbitrary waveform generator) to which the wanted laser pulse sequence is programmed to. In the successful measurement the AWG was programmed to send 20 ns pulses with 5 ns rise time at double the resonator mechanical resonance frequency for π measurement and at the mechanical resonance frequency for 2π measurement. As the resonance frequency was 1.95 MHz, meaning that the oscillation period is around 500 ns, it's clear the pulses are short compared to the oscillation period. The voltages sent from the AWG were offset so that the EOM modulates the laser intensity to be close to zero except during the pulses when the EOM would let as much of the laser intensity through as possible. In the signal arm, there is a PBS (polarizing beam splitter) right after the light comes out from the fiber to make sure that the light is as linearly polarized as it can be since the fibers can disturb the polarization.

When the light goes from the EOM to the signal branch, it is linearly polarized. To make sure that it is as linear as possible, the beam is made to go through a PBS, that only transmits horizontally polarized light and reflects to the side vertically polarized light. After that, the light goes through a PBS again with no changes in the polarization (unless it has somehow deteriorated after the last PBS). Next, the beam goes through a QWP (quarter wave plate) that is used to optimize the beam so that as much light as possible gets to the resonator and back from it to the detector. After the light has gone to the resonator and gone back through the QWP again, the light goes again through the second PBS but as the light now has a different

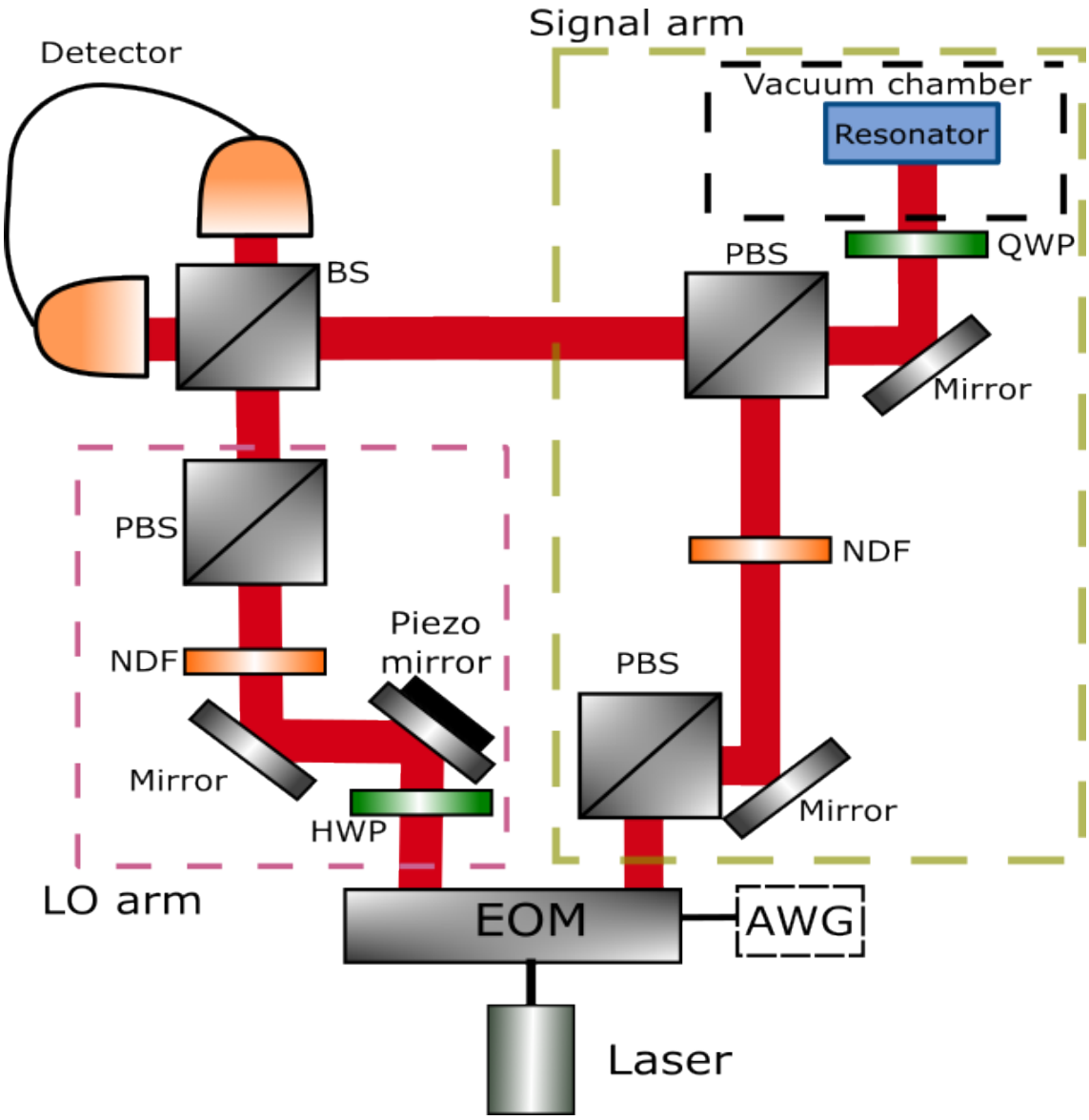

Figure 3. Simplified schematic diagram of the interferometer setup used.

polarization, it goes to the detector instead of the signal arm where it came from.

The resonator was horizontally aligned in the successful measurement which led to the resonator coupling best to horizontally polarized light. This is because the sample used could not fit the sample stage on the second measurement setup unless horizontally or vertically aligned. It would be more optimal to have the resonator be at 45° angle as if the resonator slit is aligned to be perpendicular to the polarization of the incoming light, there would be very little light going to the resonator and interacting with it, and if it were horizontally polarized, most of it wouldn't get reflected to the detector at the second PBS and instead would go back to the laser source.

The problems arising from the resonator being horizontally aligned are circumvented by having the QWP before the resonator, as it makes the horizontal light a mixture of horizontal and vertical light. Then only the horizontally polarized part of the light interacts with the resonator which nets a 50% loss of light that was sent to the resonator and that can get to the detector after interacting with the resonator. The light that interacted with the cavity gets reflected back as horizontal light and gets polarized as a combination of horizontal and vertical light again at the QWP. As the light then goes through the PBS again, another 50% of the intensity from the resonator is lost. Thus even in an ideal and otherwise lossless situation only 25% of the original light intensity sent to the resonator can reach the detector with information about the resonator's position.

In the LO arm, there is a half wave plate (HWP) and a PBS to make the light going to the interference beamsplitter as similarly polarized as the light coming from the signal arm. This is done to maximize the interference of the two beams to get a stronger signal. There is also a piezo mirror in the LO arm to control the phase of the LO arm. A piezo mirror's movement is controlled electrically and the movement can be very precise. The details regarding to phase in this measurement system are discussed in section 3.3.

After the laser has interacted with the sample it goes to interfere with the LO beam at a 50/50 beamsplitter and goes to the detector. The intensity measured by the detector next goes to a digitizer that digitizes and saves the data measured. The digitizer samples at the rate 2.5 GSample so the measurements have a good resolution. This is important, as the peaks are very short in time and height and the area under the peaks would preferably be measured with the most precision possible.

During the analysis of measured results, it was noticed that for some reason the AWG did not send the pulse sequence at same delay from the trigger pulse for every measurement. In the measurement, a trigger was programmed to go to the digitizer and AWG so that the digitizer and AWG start at the same time. While the digitizer would always reliably start measuring at the same time, the pulses sent from the AWG did not always start at the same time. This issue was troubleshooted at length with no resolution. Due to this, the voltage data of the measurements is aligned in the analysis. Since only the start time and noise floor of the voltage signal were not always at the same position, the distance in time between the peaks stayed the same during measurements this wasn't an issue. Analysis of the results will be discussed in the next section, Sec.4.1.

3.3 Measuring data with correct phase

For these measurements, the goal was to keep the phase difference between the two interferometer arms constant at $\pi/2$ (as was derived in 2.4) when there is no optomechanical coupling, so that when there is optomechanical coupling during the measurement, the measured phase difference will modulate around $\pi/2$. In an ideal setup, there would be no change in the phase difference other than from the cavity. In a real setup, however, there is some change in the phase difference between the arms from some interferometer components such as beamsplitters, and from outside noise sources. Using phase locking to try to lock the phase difference was tried, but no measurements showed signs of having measured resonator position when phase lock was used.

As phase locking didn't seem to work, a longer measurement was done where the phase difference between the arms was left to drift freely. Similar measurements to this one have been successful without phase locking [10]. As the drift was not too fast, it could be assumed that the phase stayed relatively the same during a part of this longer measurement. During this measurement, both interferometer arms were pulsed and a faster detector was used. In the analysis of this measurement, it was seen that the mechanical resonator position was indeed measured.

While the exact reason for the difference in success between these two measurements is not clear, it seems to be likely that it is due to pulsing both interferometer arms instead of just the signal arm. A similar successful measurement with no phase locking and pulsing in both arms has been done [10]. This an interesting question

that could be further investigated even if it is outside the scope of this thesis. The difference between the detector speeds is 200 MHz bandwidth on the second setup compared to 100 MHz bandwidth on the first setup is also a feasible reason, as the differences between the peak heights can be very slight. In an earlier successful measurement [10] a detector of 200 MHz speed was used to successfully measure the position, so it is possible that detectors slower than that are not fast enough to detect the phenomenon.

4 Results

As the theory and the methods underlying pulsed optomechanical measurements are now explained, in this section I move on to discuss the results of the measurements done. I will shortly explain how the measurements were done and show plots of the measurement results. In the subsection 4.1 I explain how the data was analyzed to extract the information about the resonator position quadrature amplitude and show histograms for analysis results for both measurement series done for this thesis. In the subsection 4.2 I show how the fits were done to the histograms and show how the precision of the position measurement was characterized.

Two measurement sets were done, one π measurement set and one 2π set, where one measurement is a pulse train. For both of these measurement sets, only the first 1000 measurements were used in the analysis as the phase difference between the interferometer arms was assumed to have drifted after that. A plot of a pulse train is in Fig. 4a and a detail of a peak shape is in Fig. 4b. It can be seen that the pulses are not smooth.

As mentioned before, laser pulse trains were sent to both interferometer arms. At the beginning of the measurement, there is an empty signal as the digitizer starts listening for pulses approximately 2 µs before the AWG starts to send the pulses to the EOM which modulates the laser power accordingly. Depending on if the pulse train is for a π or 2π measurement, the pulses are either sent at double the resonator's mechanical resonance frequency or at the mechanical resonance frequency. Between consecutive measurements, there is also a short rest time, partly due to the AWG's slow response to the trigger. The break between the measurements is required so that the resonator has time to thermalize. This guarantees that the previous measurement doesn't affect the next one.

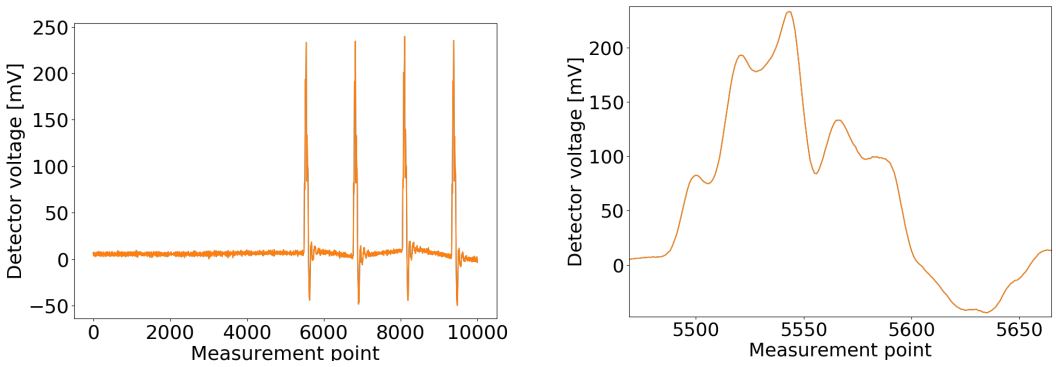

Figure 4. **a)** 2π measurement data. The peak train starts about halfway through the measurement and there are four peaks during the measurement. **b)** A zoom-in on the first peak in a).

4.1 Analysis

The aforementioned slowness of the AWG to react to the trigger caused issues in the analysis of the data, as the pulses didn't reliably start at the same time as can be seen in Fig. 5a, where 50 measurements of the analyzed measurement series are plotted. A closer study of the pulses showed that while the pulse trains might not start at the same time, the time between the pulses was still constant throughout the measurement set. To make analyzing the data more manageable, the peaks were aligned so that the first peaks were at the same points. This was done by finding the first peak of every measurement and aligning those to be at the same position for every measurement. The voltage floor drifted between measurements so the voltages were also vertically aligned to have the voltage floor be at least close to the same level between all measurements. This made the comparison of the areas under the peaks more reliable. A plot of 50 measurements where the peaks have been aligned is in Fig. 5b.

After the voltage peaks are aligned, the area under the first two peaks is calculated. There are more than two pulses in a pulse train but the first two laser pulses might have an influence on the resonator motion and hence the rest of the pulses do not measure the thermal state of the resonator anymore. Thus only the first two are used in the analysis, as they have all the necessary information about the resonator motion for quadrature amplitude extraction. The limits for data points used in the peak area calculation are found by hand for each measurement set and are separated

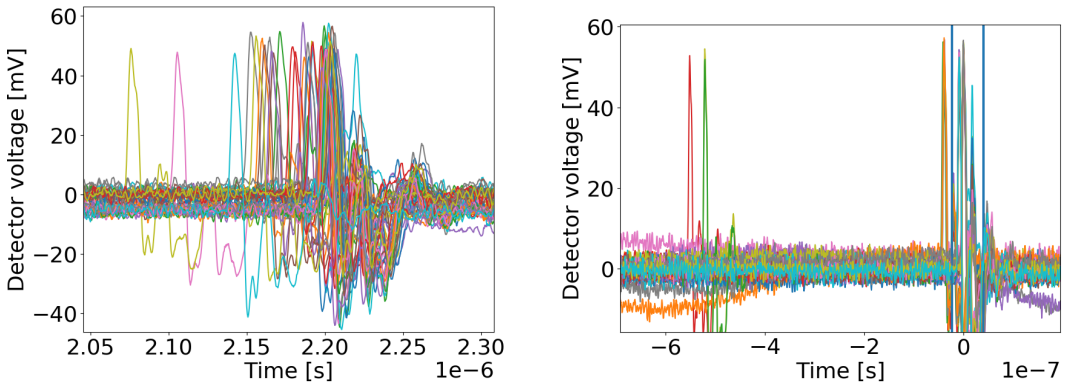

(a) **(b)**

Figure 5. a) 50 measurements plotted in the same plot without alignment. The plot is zoomed in on the first peak. **b)** 50 measurements plotted in the same plot with alignment. The time axis in the plot is so that the middle of the first peak is at 0, as this made aligning the first peaks easier. While the time axis might make it seem like this plot is zoomed in closer to the first peak, this plot has actually double the width of the plot in a). It has also been confirmed that the peaks are the same width in both plots.

by the same amount of points for both peaks i.e. both peaks are analyzed with the assumption that they are equally wide. The area under the peaks is then calculated within these limits by summing the voltage values together. As the voltage floor is aligned to be at 0 mV, this gives the area under the peak in mV units.

Following the calculation of the areas under the peaks, the areas under the first two consecutive peaks are compared by subtracting the areas and dividing the result by two to normalize the value. The result of this calculation for all the measurements is then plotted into a histogram. For the π measurement set, the histogram is expected to have two peaks as the measurement wasn't fully in the linear region whereas 2π measurement set histogram is expected to have a single peak around zero, as nonlinearity in the 2π measurement causes the histogram peak to heighten around zero.

A probability density function of the homodyne signal is fitted to the histograms if the histograms plotted have a shape that implies that the resonator position was measured. This is the case, if either both of the histograms are a single peak and the 2π histogram is narrower than the π histogram, which would mean that the measurement series were in the linear region for certain, or if the 2π histogram is a single peak but the π histogram is double-peaked on both sides of zero, meaning

that the measurement series weren't fully in the linear region. Since the successful measurement series were not in the linear region based on the π histogram shape, the probability density function of the homodyne signal defined in eq. 42 was fitted to the histograms. As the histograms from these measurement series implied that the measurement series had not been in the linear region, i.e. $\frac{2Gx(t)}{\kappa} \not\ll 1$, the signal from the resonator is expected to be a combination of a Gaussian and a nonlinear homodyne signal. The probability density function is thus

$$\begin{aligned} P(\Delta) = &\frac{1}{\sqrt{2\pi\sigma^2}}\exp\left(\frac{\Delta_+^2}{2\sigma^2}\right)\left(-\frac{1}{2S'}\left(1-\frac{1}{\sqrt{1-2S'^2}}\right)\right) \\ &+\frac{1}{\sqrt{2\pi\sigma^2}}\exp\left(\frac{\Delta_-^2}{2\sigma^2}\right)\left(-\frac{1}{2S'}\left(1+\frac{1}{\sqrt{1-2S'^2}}\right)\right) \end{aligned} \tag{62}$$

where

$$\Delta_\pm = \frac{1 \pm \sqrt{1-4S'^2}}{2S'} \tag{63}$$

is the change in the optical frequency of the cavity, σ^2 is the variance of Δ and S' is the homodyne signal divided by the normalization terms

$$S' = \frac{S}{|a_{lo}||a_{in}|\frac{4\sqrt{\kappa_{in}\kappa_{out}}}{\kappa}}. \tag{64}$$

The derivation of this function is explained in supplementary of [10].

As π and 2π measurement series were done separately, the results of the π measurement series can't be used to filter out nonlinearity from the 2π measurement series like was done in [10]. This means that the value for precision acquired in the next section is only true for the measurements that were in the linear region. Thus as the measurement precision can only be calculated from the 2π measurement, the actual imprecision of the measurement might be more than what is calculated in the next section.

4.2 Measurement results

As a result of the analysis, histograms were made for the π and 2π measurement series. These histograms are shown in Fig. 6a and Fig. 6b. In Sec. 2.4, an equation for the homodyne signal was derived in eq. 44. As mentioned before, from Fig.6a it is clear that the π measurement set had nonlinearity in it as the histogram has two peaks. The 2π measurement set in Fig.6b looks like it could be in the linear region, but this isn't necessarily true, as on cannot tell the linearity of the measurement based on only the 2π measurement.

The probability density function of the homodyne signal 62 was fitted to the histograms in Fig.6c and 6d. In the figure, the red lines are the limits of the fit. These limits need to be applied as the function that was fitted to the histograms assumes that there is no noise and in the case of the π histogram, the function is only applicable between the limits. The limits are chosen by hand to be approximately equal distance from the middle of the peak in 2π histogram or the middle of the dip in π histogram.

As can be seen from the figures 6c and 6d, the fits are good. In section 2.6 I defined the variance of a measured quadrature in eq. 57. As this quadrature was measured in the π measurement and any constant offset of the measurement was cancelled out in the analysis (as was explained in section 2.7.1), one can define x_{zpf} as

$$x_{zpf}^2 = \frac{\mathrm{Var}(X)}{2n_{th}}, \tag{65}$$

where $\mathrm{Var}(X)$ is the variance of the π measurement. As was also explained in Sec. 2.7.1, the 2π measurement only measures the shot noise of the measurement. It can be then written that the variance of the shot noise in terms of x_{zpf} is as derived in Sec. 2.6 in eq. 59

$$\sqrt{\frac{\mathrm{Var}(x_{2\pi})}{x_{zpf}^2}} = \sqrt{\frac{\mathrm{Var}(x_{2\pi})2n_{th}}{\mathrm{Var}(x_\pi)}}. \tag{66}$$

For these measurements, the number of thermal phonons during measurement was

$$n_{th} = \frac{k_B T}{\hbar\omega_m} = \frac{1.380649 \cdot 10^{-23}\ \mathrm{J \cdot K^{-1}} \cdot 293\ \mathrm{K}}{6.62607015 \cdot 10^{-34}\ \mathrm{J \cdot s} \cdot 1.951062 \cdot 10^{6}\ \mathrm{Hz}} = 3129131.418, \tag{67}$$

and inputting this result into eq. 66 among with the values for the variances of the

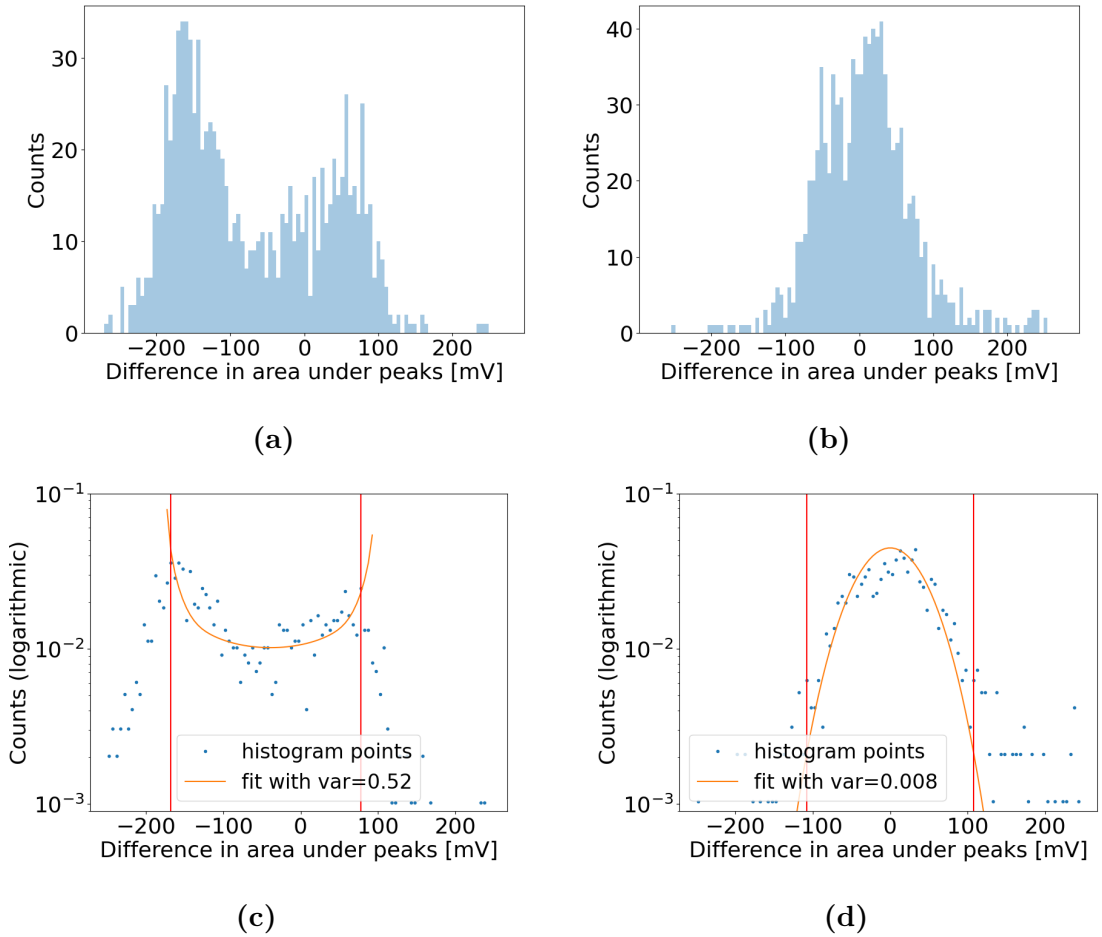

Figure 6. **a)** Histogram of the areas under two consecutive peaks in a π measurement. **b)** Histogram of the areas under two consecutive peaks in a 2π measurement. **c)** π measurement histogram with fit of eq. 62. The vertical axis of the plot is logarithmic. Red lines show fit limits. Based on the fit the variance of π measurements was 0.52 $(\mathrm{mV})^2$. **d)** 2π measurement histogram with fit of eq. 62. The vertical axis of the plot is logarithmic. Red lines show fit limits. Based on the fit the variance of 2π measurements was 0.008 $(\mathrm{mV})^2$.

2π and π measurements acquired from the fits yields the variance of the shot noise as

$$\sqrt{\frac{\mathrm{Var}(x_{2\pi})}{x_{zpf}^2}} = \sqrt{\frac{0.008}{0.52} \cdot 2 \cdot 3129131.418} = 310.29... \frac{1}{x_{zpf}} \approx 311 \frac{1}{x_{zpf}}. \tag{68}$$

The quality of this result will be discussed in the next section as well as compared with other results obtained in similar measurements done by other research groups.

5 Conclusions

Optomechanics allows for fairly simple ways to measure minuscule frequency changes of resonators among other things. Using pulsed light enables doing backaction evading measurements by allowing for one quadrature measurements that can dodge the SQL, giving way to very precise quantum measurements. One such quantum measurement is to measure the resonator's position, as was done in this thesis.

If one can build a setup where these position measurements can be done reliably with measurement error on the scale of x_{zpf}s, then it becomes possible to measure very small changes in the mechanical resonator frequency by measuring the resonator before and after the resonance change. For example, a qubit could be coupled to the resonator [20], or a mass can be placed on a resonator [21], both of which change the mechanical resonance frequency of the resonator. If one then measures the resonator with a pulsing frequency that matches the resonator's original mechanical resonance frequency, one will be able to see that the pulsed measurement histograms will have shifted due to detuning. While mass measurements using the resonance change of a nanoscale resonator were done by transducing the resonator's momentum into electric signal [21], the motion of the resonator could be measured optomechanically as well.

As pulsed measurements can resolve a frequency change via position measurements with precisions on the scale of some tens of x_{zpf}s and performing two pulsed measurement series allows for detecting fast changes with fast measurements whereas to detect the same change with continuos measurements requires one to measure for a long time, this method is relatively fast and precise compared to continuous measurements. While frequency change detection measurements weren't done for this thesis, a successful resonator position measurement was done which is the most difficult hurdle to manage in such measurements. On top of that, this was done with good precision and at room temperature, which is pretty cool in my opinion.

In this thesis, I first introduced the background of interferometric optomechanical measurements and the background of the theory behind pulsed quadrature measurements from their origins in the 1960s in Sec. 1. While these measurements originally

were interesting studies due to them being a possible way to detect gravitational waves, along the way as the research technology improved it became clear that these techniques could also be used to detect changes in nanoscale and smaller, and quantum phenomena.

For optomechanics, it is naturally important to understand the optics and the mechanics of the systems used, how the optics and mechanics couple, and what sort of quantum mechanics need to be applied. I have explained all of the concepts that are required for the reader to understand the physics of the measurements done for this thesis in Sec. 2. These concepts include the basics of cavity optomechanics, radiation pressure force and how its interactions in the cavity lead to optomechanical coupling and backaction, how the system Hamiltonian looks and how it is derived, how the aforementioned backaction can be avoided, and how the measurement precision can be found.

In Sec. 3 I have provided details on the materials and the fabrication methods used for making the nanobeam resonator. The measurement system and how it was used is explained in detail along with information about the importance of the control of the phase difference between the two interferometer arms. The information provided in the aforementioned section should be enough for the measurement to be repeatable by the reader if the reader has the equipment required.

Lastly, I have explained how the measurement results were analyzed and how this analysis indeed means that the mechanical resonator's position was measured. I have also shown in the same section how the estimation for the precision of the measurement was achieved. If the assumptions made while acquiring the estimate for the precision hold, the measurement precision is very good considering that the measurement was done at room temperature. With better optomechanical coupling a better precision should be achievable.

Overall, I have shown here that one can measure the position of a nanoscale resonator at low pressure with optomechanical pulsed measurements at room temperature. I have explained the theory behind this and given the information necessary to repeat this measurement. While the estimate obtained for the precision can't be confirmed to be fully in the linear region and thus comparable to results from other groups, if one assumes that the measurement was fully linear, then the result is fairly good. In [10] the precision for a similar measurement, where only postselected linear data was used, the precision was 58 x_{zpf} and in [9] the precision for the measurement

without any post-selection was 19 pm. In the latter paper the x_{zpf} was estimated to be around $5.7 \cdot 10^{-15}$ m, so their precision in terms of x_{zpf} is around 3333.333... x_{zpf}.

Now that the resonator position can indeed be measured the next step is to try and do a frequency change measurement. Such measurements are used to see very small changes in the resonance frequency of the resonator, useful for measuring spin coupling or small masses for example. If one gets this sort of pulsed measurement to reliably measure a resonator's position before and after the resonance frequency changes, then one can measure this frequency change very fast and very precisely. Future uses for these sorts of measurements are for example in measuring very small masses or neutral masses, such as viruses [22] or single proteins [23], with better resolution than before. Neutral mass spectroscopy via nanoresonators is also useful for nuclear physics, as the technique is blind to charge. Where one would see multiple peaks in a time of flight mass spectrometry due to charge states, only one peak is seen with nanomechanical resonators [24].

References

[1] V. B. Braginsky and A. B. Manukin. “Pondermotive Effects of Electromagnetic Radiation”. In: *Sov. Phys. JETP* 25 (4 1967).

[2] V. B. Braginsky, A. B. Manukin, and M. Y. Tikhonov. “Investigation of Dissipative Pondermotive Effects of Electromagnetic Radiation”. In: *Sov. Phys. JETP* 31 (5 1970).

[3] V. B. Braginsky and Y. I. Vorontsov. “Quantum-mechanical limitations in macroscopic experiments and modern experimental technique”. In: *Soviet Physics Uspekhi* 17.5 (1975), p. 644. DOI: 10.1070/PU1975v017n05ABEH004362. URL: https://dx.doi.org/10.1070/PU1975v017n05ABEH004362.

[4] C. M. Caves. “Quantum-Mechanical Radiation-Pressure Fluctuations in an Interferometer”. In: *Phys. Rev. Lett.* 45 (2 1980), pp. 75–79. DOI: 10.1103/PhysRevLett.45.75. URL: https://link.aps.org/doi/10.1103/PhysRevLett.45.75.

[5] K. S. Thorne et al. “Quantum Nondemolition Measurements of Harmonic Oscillators”. In: *Phys. Rev. Lett.* 40 (11 1978), pp. 667–671. DOI: 10.1103/PhysRevLett.40.667. URL: https://link.aps.org/doi/10.1103/PhysRevLett.40.667.

[6] V. B. Braginsky, Y. I. Vorontsov, and F. Y. Khalili. “Optimal quantum measurements in detectors of gravitation radiation”. In: *JETP Lett. (USSR) (Engl. Transl.); (United States)* 27.5 (Mar. 1978). URL: https://www.osti.gov/biblio/6920552.

[7] M. T. Jaekel and S. Reynaud. “Quantum Limits in Interferometric Measurements”. In: *Europhysics Letters* 13.4 (1990), p. 301. DOI: 10.1209/0295-5075/13/4/003. URL: https://dx.doi.org/10.1209/0295-5075/13/4/003.

[8] M. R. Vanner et al. “Pulsed quantum optomechanics”. In: *Proceedings of the National Academy of Sciences* 108.39 (2011), pp. 16182–16187. DOI: 10.1073/pnas.1105098108. eprint: https://www.pnas.org/doi/pdf/10.1073/pnas.1105098108. URL: https://www.pnas.org/doi/abs/10.1073/pnas.1105098108.

[9] M. R. Vanner et al. “Cooling-by-measurement and mechanical state tomography via pulsed optomechanics”. In: *Nature Communications* 4.1 (2013), p. 2295. ISSN: 2041-1723. DOI: 10.1038/ncomms3295. URL: https://doi.org/10.1038/ncomms3295.

[10] J. T. Muhonen et al. “State Preparation and Tomography of a Nanomechanical Resonator with Fast Light Pulses”. In: *Phys. Rev. Lett.* 123 (11 2019), p. 113601. DOI: 10.1103/PhysRevLett.123.113601. URL: https://link.aps.org/doi/10.1103/PhysRevLett.123.113601.

[11] Y. Liu et al. “Coherent memory for microwave photons based on long-lived mechanical excitations”. In: *npj Quantum Information* 9.1 (2023), p. 80. ISSN: 2056-6387. DOI: 10.1038/s41534-023-00749-x. URL: https://doi.org/10.1038/s41534-023-00749-x.

[12] R. Leijssen. “Measuring mechanical motion using light confined at the nanoscale”. PhD thesis. AMOLF, 2017.

[13] G. Grynberg, A. Aspect, and C. Fabre. *Introduction to Quantum Optics : From the Semi-classical Approach to Quantized Light*. Cambridge University Press, 2010. ISBN: 9780521551120. URL: https://search.ebscohost.com/login.aspx?direct=true&db=e000xww&AN=329391&site=ehost-live.

[14] B. E. A. Saleh and M. C. Teich. *Fundamentals of Photonics*. Newark, UNITED STATES: John Wiley & Sons, Incorporated, 2019. ISBN: 9781118770092. URL: http://ebookcentral.proquest.com/lib/jyvaskyla-ebooks/detail.action?docID=5720845.

[15] M. Aspelmeyer, T. J. Kippenberg, and F. Marquardt. “Cavity optomechanics”. In: *Rev. Mod. Phys.* 86 (4 2014), pp. 1391–1452. DOI: 10.1103/RevModPhys.86.1391. URL: https://link.aps.org/doi/10.1103/RevModPhys.86.1391.

[16] G. J. Bowen Warwick P. and Milburn. *Quantum Optomechanics*. Boca Raton: CRC Press, 2015. ISBN: 9780429159312. DOI: https://doi.org/10.1201/b19379.

[17] R. Leijssen and E. Verhagen. "Strong optomechanical interactions in a sliced photonic crystal nanobeam". In: *Scientific Reports* 5.1 (2015), p. 15974. ISSN: 2045-2322. DOI: 10.1038/srep15974. URL: https://doi.org/10.1038/srep15974.

[18] R. Leijssen et al. "Nonlinear cavity optomechanics with nanomechanical thermal fluctuations". In: *Nature Communications* 8.1 (2017), ncomms16024. ISSN: 2041-1723. DOI: 10.1038/ncomms16024. URL: https://doi.org/10.1038/ncomms16024.

[19] Z. Diao et al. "Stiction-free fabrication of lithographic nanostructures on resist-supported nanomechanical resonators". In: *Journal of Vacuum Science & Technology B* 31.5 (Sept. 2013), p. 051805. ISSN: 2166-2746. DOI: 10.1116/1.4821194. eprint: https://pubs.aip.org/avs/jvb/article-pdf/doi/10.1116/1.4821194/13486761/051805_1_online.pdf. URL: https://doi.org/10.1116/1.4821194.

[20] A. D. O'Connell et al. "Quantum ground state and single-phonon control of a mechanical resonator". In: *Nature* 464.7289 (Apr. 2010), pp. 697–703. ISSN: 1476-4687. DOI: 10.1038/nature08967. URL: https://doi.org/10.1038/nature08967.

[21] J. Chaste et al. "A nanomechanical mass sensor with yoctogram resolution". In: *Nature Nanotechnology* 7.5 (2012), pp. 301–304. ISSN: 1748-3395. DOI: 10.1038/nnano.2012.42. URL: https://doi.org/10.1038/nnano.2012.42.

[22] S. Dominguez-Medina et al. "Neutral mass spectrometry of virus capsids above 100 megadaltons with nanomechanical resonators". In: *Science* 362.6417 (2018), pp. 918–922. DOI: 10.1126/science.aat6457. eprint: https://www.science.org/doi/pdf/10.1126/science.aat6457. URL: https://www.science.org/doi/abs/10.1126/science.aat6457.

[23] M. S. Hanay et al. "Single-protein nanomechanical mass spectrometry in real time". In: *Nature Nanotechnology* 7.9 (Sept. 2012), pp. 602–608. ISSN: 1748-3395. DOI: 10.1038/nnano.2012.119. URL: https://doi.org/10.1038/nnano.2012.119.

[24] E. Sage et al. “Neutral particle mass spectrometry with nanomechanical systems”. In: *Nature Communications* 6.1 (Mar. 2015), p. 6482. ISSN: 2041-1723. DOI: 10.1038/ncomms7482. URL: https://doi.org/10.1038/ncomms7482.